DESIGN OF ADAPTIVE CONTROLLER TO IMPROVE STABILITY FOR ELECTRIC VEHICLES

Le Dinh Hieu*

School of Engineering and Technoloy - Hue University, Vietnam

*Corresponding author: ledinhhieu@hueuni.edu.vn

(Received: July 16, 2024; Revised: August 11, 2024; Accepted: September 26, 2024)

DOI: 10.31130/ud-jst.2024.336

Abstract - Currently, with outstanding advances in automated driving technology, modern vehicles with a variety of electronic control systems help improve traffic safety. One is the electronic stability adaptive control system that ensures the electric vehicle stays on track even in unpredictable situations such as driving on slippery roads, sudden movements, and changing direction of driving on the highway. The article focuses on developing an adaptive electronic stability controller for electric cars modelled on software Matlab-Simulink. Design a vehicle stability controller within the scope of surveying the slippage of four tyres in the stability limit ellipse corresponding to the driving angle when using a fuzzy adaptive electronic stability controller (Fuzzy-ESC) compared to compared with the electronic stability control swarm optimization controller (PSO-ESP), it minimizes skids and vehicle rollovers during obstacle avoidance, lane changing, corner entry/exit and sudden acceleration.

Key words - Electronic stability control (ESC); Electronic Stability Programs (ESP); Fuzzy-ESC; PSO-ESP; Active safety control systems; EVs.

1. Overview of electronic stability control for electric vehicle

Nowadays, every new car on the market has many electronic control systems serving many different purposes. The focus of the control systems is to ensure the safety of electric vehicles (EVs) when operating on the road. As we know, sometimes the driver loses concentration and sometimes makes mistakes, but when driving a car, it does not allow any mistakes that lead to serious consequences and are related to human life [1]. Automatic control systems help the driver to handle dangerous situations that the driver cannot handle by himself due to loss of concentration or sudden changes that human psychology cannot respond to in time [2-5].

The electronic stability control system is also known by many different names such as ESP (Electronic Stability Program) [2] or DSC (Dynamic Stability Control), ESC (Electronic Stability Control) [3], depending on the car manufacturer's name for this system. The control system can detect loss of steering control and resolve it by applying braking torque to each wheel, and some manufacturers integrate an additional engine power management function. In addition, the electronic stability control helps the car avoid oversteer or understeer.

The technology of the electronic stability control system is based on the ABS (Anti-Locking Brake System), which allows the system to break each wheel individually. Even the TCS (Traction Control System) often acts as a secondary function of the ESP. However, compared to the ABS and the TCS that improve the car's ability to turn, the ESP system itself helps reduce the loss of control of the car's steering.

Regarding the effectiveness of the ESP controller, the US National Highway Traffic Safety Administration published a study in 2006, that the use of ESP reduces fatal vehicle crashes by 35% for cars and 67% for family sport utility vehicles (SUVs), data provided from various studies referred to in [3]. ESP systems have been mandatory on all passenger vehicles in the United States since 2012 and in the European Union since 2014.

The decision algorithms of ESP mainly have the following forms: PID feedback control, neural network control and optimal control [1]. The paper [2] used the AFSA and SA methods to update the PID parameters to control the ESP system to change the direction of the truck at the expected yaw velocity. The robust fuzzy controller [3-8], the optimal stabilization based on parallel distribution compensation was designed using the Takagi–Sugeno fuzzy model of electric vehicles with the fuzzy model stability feedback gain, optimizing the longitudinal velocity state stability control parameters for automobiles [6]. Parameter optimization of intelligent controllers [9] and fuzzy sliding mode controller (FSMC) were proposed to solve the instability caused by nonlinear characteristics when turning or changing lanes at high speeds [10]. Fast online parameter estimation of the vehicle's cornering stiffness coefficient using deep learning algorithms to control the state stability of automobiles [11].

The main purpose of this paper is to develop an electronic stability control algorithm for automobiles with a nonlinear dual-track model. The ESP algorithm is used to control the stability of the vehicle by applying braking torque, so it may not be able to maintain the longitudinal speed of the vehicle, so it needs to be improved to increase stability [1]. For the above reason, the cruise control algorithm can be added to work with ESP, so it is called enhanced stability control ESC, with the above approach, it is possible to avoid using two different control systems at the same time on the automobile. Furthermore, ESC controls the torque for each individual wheel [5], so the proposed research topic to improve the control quality applies modern algorithms such as adaptive fuzzy control, multi-objective optimization algorithm PSO [6].

2. Dynamics Equation of Electric Vehicles

2.1. The twin-track model of EVs

2.1.1. Modelling the system on a dual track model

The vehicle dynamic model is divided into four parts: chassis, transmission, drive system and body, as shown in

Figure 1. In the model shown in Figure 1, the parameters: drive torque M_m (Nm), brake torque M_b (Nm) and regenerative brake torque M_b (Nm) on each wheel and the steering angle δ of the two front wheels (with the same magnitude) are selected as inputs to the steering system or to the control system. In addition, the model also takes into account external disturbances. Survey and model the road surface on which the car moves with different roughness, leading to different values of the coefficient of friction μ between the tyres and the road surface [7]. The impact of wind is also modelled by the torque acting on the body when the car moves.

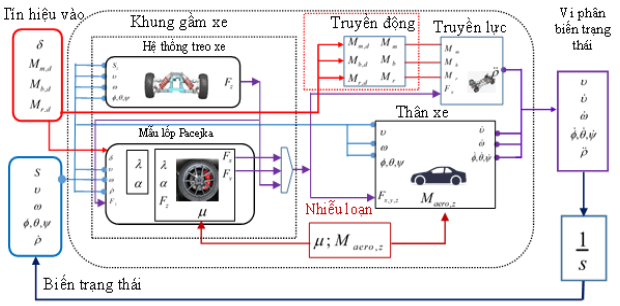

Figure 1. *Diagram of the dual track model*

The nonlinear dual-track model [2] of an electric vehicle is used for investigation in Figure 1, which represents the actual states of the vehicle when operating on the road.

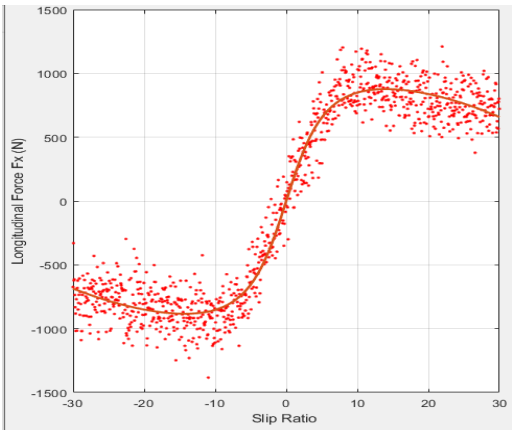

Figure 2. *Data on tyre lateral forces*

Modelling the lateral forces of tyres when moving on the road used to investigate electric cars is shown in Figure 2.

2.1.2. The balanced elliptical model of the tire

The tire model describes the tire contact surface with a relatively small area directly interacting with the road surface; through two important variables: the slip coefficient λ and the lateral slip angle α (rad) [11, 12]. Each tire of the wheel is described by the following correlation equation [13]:

$$\lambda_i = \frac{r \cdot \dot{\rho}_i - v_{x,i}}{\max\left(\left|r \cdot \dot{\rho}_i\right|, \left|v_{x,i}\right|\right)} \quad (1)$$

$$\alpha_i = \arctan\left(\frac{v_{y,i}}{\left|v_{x,i}\right|}\right) \quad (2)$$

Where: r is the wheel radius (m), $v_{y,i}$ is the angular velocity (rad/s) of the i-th wheel, $v_{x,i}$ (rad/s) and $v_{y,i}$ (rad/s) are the speeds of the *i-th* wheel-center of the wheel along the *x* and *y* axes respectively.

The mathematical model of Pacejka [8] to model the interface between the tyre and the road surface with the shape factor parameters, two input parameters λ, α (with λ: slip coefficient and α: lateral slip angle). Pacejka's mathematical formula approximately describes the characteristics of important forces and moments generated at the contact area between the tyre and the road surface, including longitudinal force, and lateral moment. While the slip coefficient is used to calculate the longitudinal force, and lateral force [14], the lateral moment is a function of the lateral slip angle α of the tyre. For the input slip variable x and shape factors A, B, C, and D; the formula in its most basic form to calculate the force F_L (N) is as follows [13, 15, 18]:

$$F_L = A \cdot \sin\left[C \cdot \arctan\left(B_x - D\left(B_x - \arctan(B_x)\right)\right)\right] \quad (3)$$

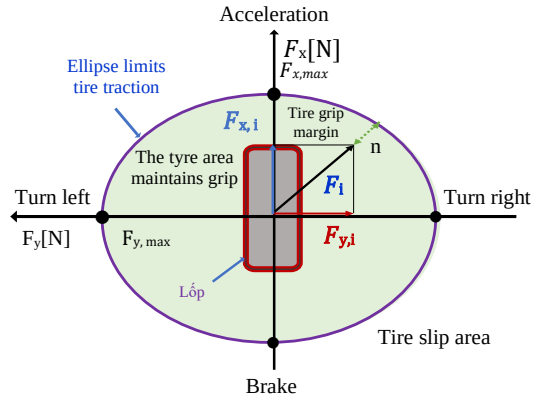

Figure 3. *Traction ellipse of EVs tires*

The paper applies the combined slip method with the friction ellipse used described in detail [16], and shows the dependence of the longitudinal and lateral forces of the tire described by the Kamm circle [17], also known as the traction circle or friction circle. The longitudinal force F_x (N), the lateral force F_y (N) and the normal force F_z (N), the friction coefficient μ are then constrained by the following inequality:

$$\sqrt{F_x^2 + F_y^2} = \mu \cdot F_z \quad (4)$$

However, the practice and the model (4), one considers an ellipse instead of a circle and the ellipse is described by the following inequality:

$$\frac{F_x^2}{F_{x,\max}^2} + \frac{F_y^2}{F_{y,\max}^2} \le 1 \quad (5)$$

If the expression of F_x (N) and F_y (N) on the left side of equation (5) ≤ 1, the tyre still maintains its grip on the road surface. On the contrary, if the result of the expression on the left side of (5) >1, the tyre will lose its grip on the road surface and slip. The ellipse representing the tyre traction limit is shown in Figure 3.

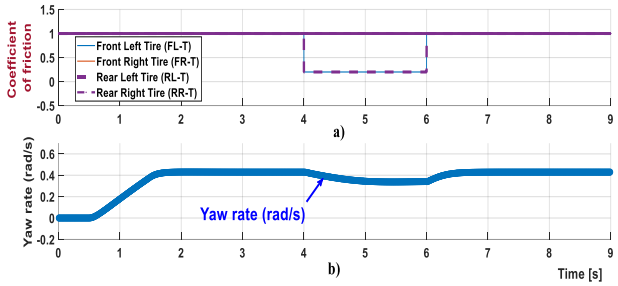

Figure 4. *Investigation of the friction coefficient μ perturbation for both left tyres of the EVs*

The coefficient of friction μ from equation (4) is assumed to be equal to 1 in the usual case with a fairly sticky road surface. Reducing its value independently for each wheel simulates driving on a slippery road, which μ is considered a variable causing external disturbances to the EVs, as shown in Figure 1. The effect of μ is determined by simulation with the situation where the car starts to turn left with a constant yaw angular velocity and a constant longitudinal velocity at the centre of gravity of the EVs V_C . At that time, the road surface μ at the two left wheels suddenly decreased to μ=0.2, leading to a decrease in the yaw ratio, causing the driver to understeer a little, as shown in Figure 4. The Figure 4.a) shows that the friction coefficient is equal to 1 and then decreases to 0.22. At the time from 4-6(s), the velocity along the Yaw axis changes from 0.4(rad/s) at time 4(s) and decreases to 0.35(rad/s), then recovers to 0.4(rad/s) at time 6.4(s).

2.2. The equation describing the body of EVs

Another important part of the dual-track model is the equations describing the vehicle body. Since it is modelled, the EVs use Newton-Euler equations, which have the following general vector form:

$$J\dot{\omega}+\omega\times(J\omega)=M \tag{6}$$

Where: J (kg.m^2) is the moment of inertia matrix of the vehicle body, ω (rad/s) is the angular velocity vector of the vehicle body and M (Nm) is the moment vector. The right side of equation (6) is rewritten as:

$$J\dot{\omega}+\omega\times(J\omega)=\sum_{i=1}^{4} r_i\times F_i+M_A \tag{7}$$

Where: r_i (m) is the position vector of the centre of the *i-th* wheel and F_i (N) is the vector of forces acting on the *i-th* wheel; M_A is the vector of external torques caused by aerodynamic forces.

While the first two elements of the vector ($r_i\times F_i$) are always considered to be zero, the third element is an aerodynamic torque disturbance acting inward (7) and Figure 1.

2.3. Transmission driver systems

In EVs, to save energy, increase efficiency, reduce energy consumption, occupy less space, be light in weight, and require less maintenance [15], the permanent magnet rotor synchronous motor (PMSM) is one of the suitable solutions chosen as the main drive motor for each wheel. The PMSM drive system drives the main, braking torque, and regenerative braking torque for each wheel [14] and is modelled by the following equation:

$$J_i\ddot{\rho}_i=M_{m.i}-M_{b,i}-M_{r,i}-r\cdot F_{x,i} \tag{8}$$

Where: J_i (kg.m^2) is the moment of inertia of the *i-th* wheel and $\ddot{\rho}_i$ (rad/s) is angular velocity. $M_{m.i}$(Nm), $M_{b,i}$(Nm) and $M_{r,i}$(Nm) are the main driving torque, braking torque and regenerative braking torque acting on the *i-th* wheel, respectively, r (m) is the wheel radius and $F_{x,i}$ (N) is the longitudinal force acting on the *i-th* wheel. In the paper, only forward motion is considered so the torque is always positive to satisfy equation (8).

In the implementation of the torque limit simulation actuator from equation (8), we have the torque required from the driver or the control system as input. The modelling of the drive system needs to ensure the accuracy between the numerical simulation and the real physical drive system, so the input signal saturation and delay model have been added to the modelling of the control system.

The PMSM motor chosen as the drive device for each wheel has an upper limit of the driving torque saturation with the *i-th* wheel: $M_{m.d,i}$ (Nm) is determined by the maximum torque $M_{m.\max}$ (Nm) or by the maximum power $P_{m,\max}$ (kW) [5], depending on the angular velocity of the *i-th* wheel $\dot{\rho}_i$, according to the equation:

$$M_{m.d,i}=\frac{P_{m,\max}}{\dot{\rho}_i} \tag{9}$$

Assuming the speed limit of the dual carriageway model is $v_m(m/s)$, $P_{m.\max}$ (kW) can be calculated using the drag equation as follows:

$$P_{m.\max}=\frac{1}{2}\rho\cdot C_D\cdot A\cdot v_m^3 \tag{10}$$

Where: ρ is the air density, C_D is the drag coefficient and A is the frontal area of the vehicle (m^2) when substituting the values into (2.10) and we can calculate $P_{m,\max}(kW)$ and $M_{m.\max}(N\cdot m)$.

The required braking torque is divided into two branches if regenerative braking is used. The regenerative braking will satisfy the demand as much as possible by saturating it within its limits. Then, the saturation signals will be subtracted from the required braking torque, and fed into the classical braking system with the upper saturation limit being $M_{b.\max}(N\cdot m)$.

Regenerative braking is essentially a vehicle-driven electric motor that turns into a generator in the event of a downhill situation. So instead of applying driving torque to the wheels, the wheels will rotate the motor themselves and convert the kinetic energy of the wheels into electrical energy stored back into the vehicle's battery. Applying braking torque to the wheels is because the wheels lose kinetic energy. Regenerative braking is much

more regenerative than using conventional braking, as it not only recovers the used energy but also does not pollute the environment, unlike conventional braking, which releases microscopic wear particles during braking [6]. The upper saturation limit of the required regenerative braking torque is similar to that of the motor, but only takes into account 40% of $M_{m.\max}$ and $P_{m,\max}$ due to its efficiency. Furthermore, at low speeds, the regenerative braking torque is further limited [7] and the saturation of the regenerative braking torque is shown in Figure 5.

The delay of each actuator can be modelled by a first-order transfer function as follows:

$$G(s) = \frac{1}{\tau \cdot s + 1} \quad (11)$$

Where: τ is the time constant, the magnitude represents the delay. The electrical time constant 2(ms) is chosen for the main driving electric motor of the drive system, while the mechanical time constant of the drive system is included in the wheel inertia moment model. The time delay of the braking system is slightly larger, so its time constant is set to 22(ms).

3. Development of EV stability control algorithm

3.1. Design of reference model EVs

The reference signal set is designed to select appropriate reference signals from the model for the control system. In addition to the vehicle speed deviation and yaw angle deviation generated by both the vehicle kinematic model and the data lookup from the parameter table, the vehicle speed along the body at V_{CG} is input.

The control signal is based on the magnitude of the vehicle speed measured from the dual-track model, the reference controller will automatically select the "appropriate speed deviation" and yaw angle of the vehicle. When the vehicle drives forward at a speed within the range $0 \div 0.5(m/s)$, the signals are fed back from the vehicle kinematic model. Conversely, at the vehicle speed $v_x > 0.5(m/s)$, the vehicle kinematic model is taken from the model parameters as shown in Figure 5.

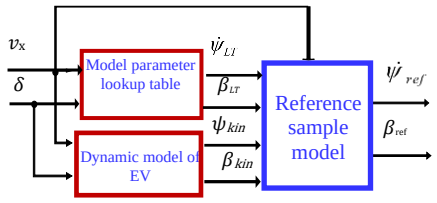

Figure 5. *Signal reference diagram of the EVs model*

3.2. The PSO-ESP adaptive controller

The PSO-ESP adaptive electronic stability controller applies the PSO feedback optimization algorithm based on the increase or decrease of the torque bias, which is achieved by applying braking torque to both left and right wheels. Since the torque bias rate is the only quantity measured and implemented for vehicles with a propulsion system, regenerative braking cannot be used. The torque bias is measured from the dual-track model and subtracted from the reference deviation from the vehicle model to the PSO adaptive swarm controller. If the generated torque bias is positive, the required braking torque is equal to the torque that would be applied to both left wheels of the vehicle. On the other hand, if the generated torque bias is negative, it is multiplied by -1, which turns it into the required braking torque applied to both right wheels of the vehicle. The logic block is depicted in Figure 6 and is limited in its implementation by saturation blocks (Positive, Negative).

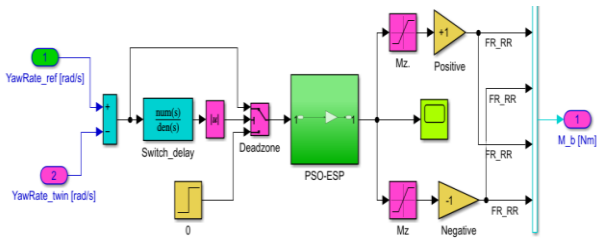

Figure 6. *Modelling of the PSO-ESP adaptive swarm controller of the cabinet electrical balance system on Simulink*

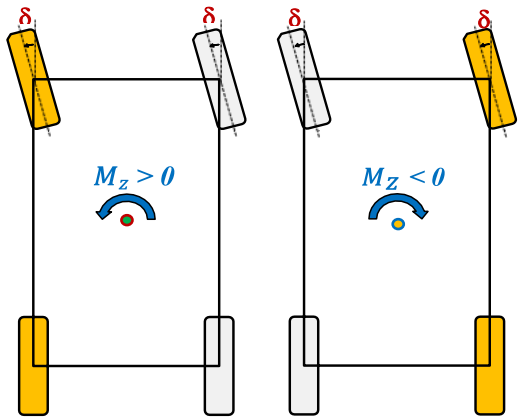

Figure7. *Principle of PSO-ESP controller*

An energy function that takes PI parameters as input values and returns the energy value of the PI-driven model as its output has the format:

The optimization problem is described in terms of energy functions and the goal of the optimization algorithms is to minimize the value of the objective function [20]:

$$F = (1 - exp(-\beta)).(M_p + E_{ss}) + exp(-\beta).(T_s - T_r) \quad (12)$$

$$F = (1 - e^{-\beta}).(M_P + E_{SS}) + e^{-\beta}.(T_s - T_r)$$

where: F: Fitness objective function; M_p: Peak crossing; T_s: Setup time; T_r: Rise times, and β: Scaling factor (it depends on the designer's choice). We take the scaling factor $\beta = 0.5$ and E_{ss} is calculated as follows:

$$E_{ss} = 1/(1 + dcgain(Model\_Vehicle)) \quad (13)$$

$$Objective\ function\ [F] = Fittness(K_p, K_i) \quad (14)$$

Since the PSO-ESP controller is not always active and only intervenes when it detects a significant loss of steering control of the vehicle [15], a dead zone is added. When the PSO-ESP has an absolute value of the difference between the measured yaw rate and the reference yaw rate lower than $\Delta\psi_{ESP} = 0.035(rad/s)$, and instead sets the required braking torque to zero.

The first requirement is that the control system must react promptly when the steering control is lost, which will help to minimize the deviation value. However, a lower value will make the PSO-ESP transition too frequent, which is difficult to implement in practice, so the $\tau_{min} = 1(ms)$ delay is added to the control process to reduce the transition and make it easier to apply. The deviation torque generated $M(Nm)$ from the braking torque applied to one front wheel and one rear wheel on the same side of Figure 7.

3.3. Electronically stabilized Fuzzy logic controller (Fuzzy-ESC)

The Fuzzy-ESC (Fuzzy logic - Electronic stability control) controller, applies an intelligent algorithm to independently control each wheel torque. Compared with the Fuzzy-ESC stability controller [16-18]. The Fuzzy-ESC controller is always active because it not only controls the braking torque but also the transmission torque. Adaptive electronic stability controller includes the function of both Fuzzy-ESC cruise control regenerative braking system and angular velocity controller of each wheel.

First, perform the conversion of the longitudinal speed of the vehicle body at V_C to the longitudinal speed of each wheel on the fixed frame of the vehicle body. Perform the next conversion of the longitudinal speed to the fixed frame with the car wheel to simplify, with a small steering angle, this conversion has almost no impact on the system. If V_{C,V_x} is the longitudinal speed at V_C and W_{i,V_x} is the longitudinal speed of the *i-th* wheel in the fixed frame of the vehicle body, then for the reference signal as follows:

$$W_{i,V_{x,ref}} = V_{C,V_{x,ref}} - s_{tr} \cdot \dot{\psi}_{ref} \quad (15)$$

$$W_{i,V_{x,ref}} = V_{C,V_{x,ref}} + s_{ph} \cdot \dot{\psi}_{ref} \quad (16)$$

With $i \in \{1, 3\}$.

When $i \in \{2, 4\}$, where s_{tr} and s_{ph} are the horizontal distances from V_C to the left and right wheels, respectively.

The same applies to the measured signals from the dual-track model, when we equal all the indices of the reference model in equations (15) and (16) to *ref* represent the instantaneous variable state of the system, we now represent it as Figure 9.

The controller is applied to each wheel. Where $W_{i,V_x} - W_{i,V_{x,ref}} = e$ and the deviation e are fed into the fuzzy logic controller, the output signal of the proportional controller gives the slip ratio λ_i. The slip ratio is then saturated with the lower limit $\lambda_{i,min} = -0.1$ and the upper limit $\lambda_{i,max} = 0.1$. Depending on $W_{i,V_{x,m}}$ and $\dot{\rho}_{i,m}$, the measured angular velocity of the *i-th* wheel is calculated, the reference angular velocity is calculated for further control, and the calculation is derived from equation (1).

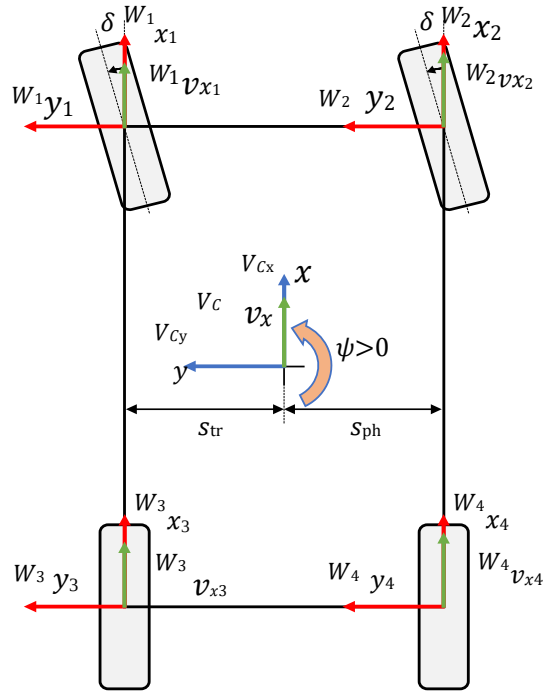

Figure 8. *Transformation of the coordinate system from the four tyres to the centre of the EV*

If $W_{i,V_{x,m}} \le r \cdot \dot{\rho}_{i,m}$ (r (m) is the radius of the wheel) and $W_{i,V_{x,m}} \ge 0$, then we have the following expression:

$$\dot{\rho}_{i,ref} = \frac{W_{i,V_{x,m}}}{r(1-\lambda_i)} \quad (17)$$

Conversely, if $W_{i,V_{x,m}} > r \cdot \dot{\rho}_{i,m}$ and $W_{i,V_{x,m}} \ge 0$, then we have the following expression:

$$\dot{\rho}_{i,ref} = \frac{(1-\lambda_i) \cdot W_{i,V_{x,m}}}{r} \quad (18)$$

We consider the forward direction of the vehicle so the equations for $W_{i,V_{x,m}} \ge 0$, the two equations (15) and (16) differ only in the plus and minus signs. The measured angular velocity of each wheel is then subtracted from its reference value from the sample model.

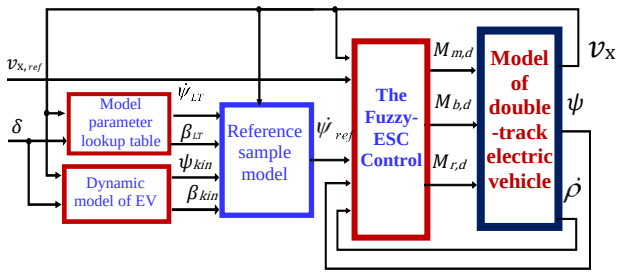

Figure 9. *Schematic of the Fuzzy-ESC intelligent controller*

Using the Fuzzy logic control applied to the closed-loop controller [16]. When the output signal of the fuzzy logic controller is positive, it represents the required driving torque. On the other hand, if the output signal of the fuzzy logic controller is negative, it is the required braking torque. Therefore, the output signal of the fuzzy logic controller is multiplied by -1 before being transmitted to the regenerative braking system or braking system as

shown in Figure 11. The intelligent Fuzzy-ESC controller is shown in Figure 12.

Design the membership functions of the fuzzy association rule [16] as shown in Figure 10, Figure 11.

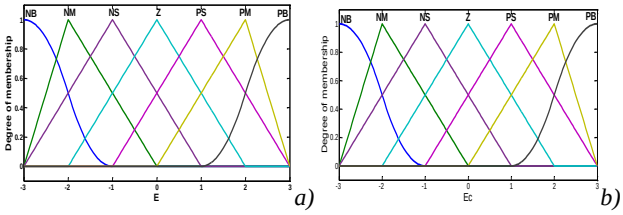

Figure 10. *Input fuzzy membership functions: a) E and b) Ec. NB (Negative); NM (Medium); NS (Small); Zero; PS (Positive); PM (Positive); PB (Positive)*

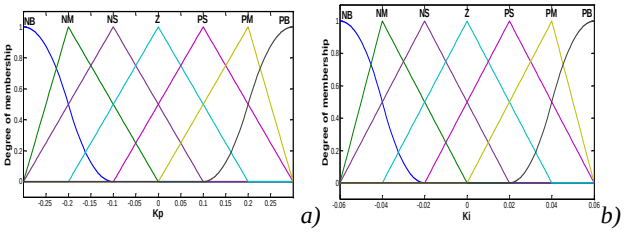

Figure 11. *The Output fuzzification function: a) Kp; b) Ki*

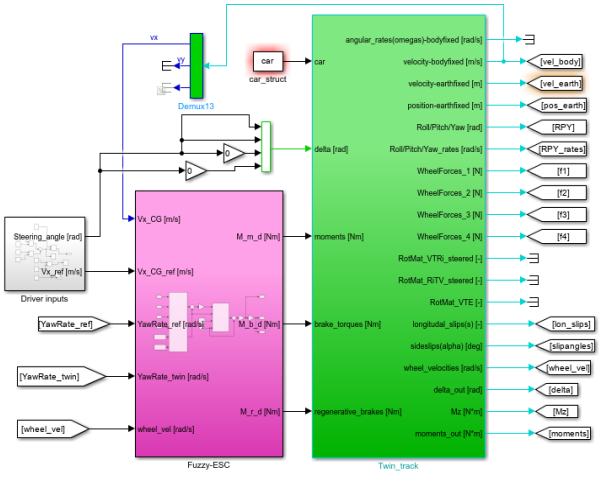

Figure 12. *Modelling of the Fuzzy-ESC electronically stabilized fuzzy controller on Simulink*

The membership functions of the Mandani Fuzzy controller for the input map the speed error (E) and the proportional error (Ec) to the membership degree [-3, 3], while the membership functions for the output play the opposite role. There are seven linguistic variables, namely Positive Large (PL), Positive Medium (PM), Positive Small (PS), Zero (ZO), Negative Small (NS), Negative Medium (NM), Negative Large (NL). The input and output fuzzification functions designed in the paper are depicted as Figure 10 and Figure 11, respectively. They include triangular and sigma membership functions. The output of the Fuzzy logic controller will optimize the controller parameters, and the controller output will continue to provide input control signals to the ESC. Model the Fuzzy-ESC controller in Figure 12. Simulation and evaluation results.

Survey and evaluate the response of the controllers corresponding to the steering signals acting on the vehicle in incident situations such as avoiding obstacles, changing lanes, falling asleep, etc. as Figure 13 [9]. Vehicle parameters of the EVs is used to simulate and evaluate the quality of the controllers according to [10].

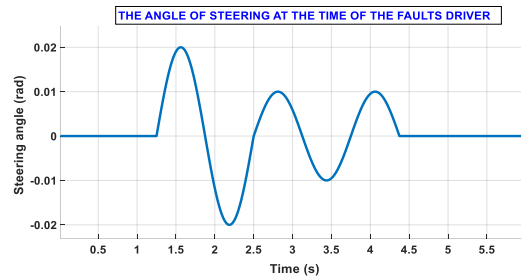

Figure 13. *The angle of steering at the time of the fault driver*

3.4. EVs with PSO-ESP controller

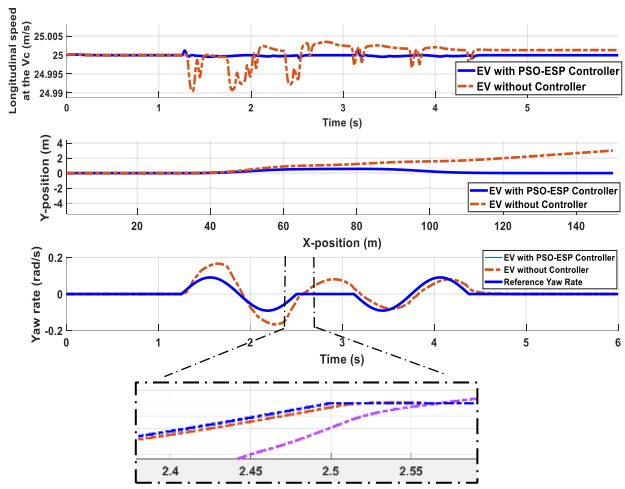

Figure 14. *Evaluation of the impact of the vehicle with PSO-ESP controller compared with the vehicle without controller*

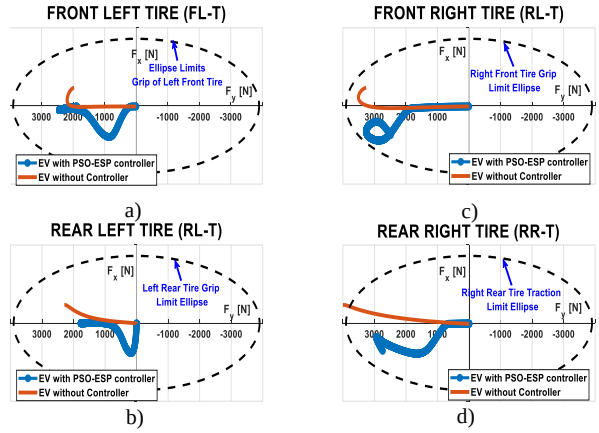

Figure 15. *Forces act on each tyre when the vehicle applies the PSO-ESP controllet*

The characteristics of the PSO-ESP controller help stabilize the vehicle, but the vehicle cannot maintain the initial longitudinal speed because the PSO-ESP controller acts on an active variable, the braking torque. Although the difference in the yaw rate between the vehicle with PSO-ESP controller and the vehicle without controller is not much, the graph showing the vehicle trajectory really reflects the impact of the PSO-ESP controller. For the tire force, there is only the force in the time period of

1.25(s)÷1.88(s), corresponding to the first left turn.

Furthermore, the simulated slip coefficient and side-slip angle are shown in Figure 14 and Figure 15, respectively. Figure 15 shows that the PSO-ESP controlled vehicle keeps all four tires within the tire grip zone with smaller layer oscillations than the vehicle without the controller. Tire number four slips and goes beyond the tire grip limit ellipse for the vehicle without the electronic stability control, Figure 15 d.

Comparison of the vehicle with only the PSO-ESP controller and the EVs without the controller. The black dashed line is the traction ellipse, as shown in Figure 14 and Figure 15.

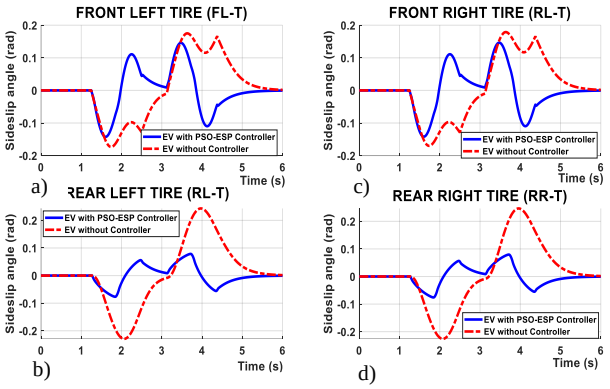

Figure 16. *Comparison of the sideslip angle of the vehicle with PSO-ESP controller and vehicle without the controller*

3.5. EVs with Fuzzy-ESC controller

The Fuzzy-ESC controller stabilizes the vehicle, the vehicle maintains the initial longitudinal speed due to the Fuzzy-ESC controller acting on the active variable of the drive torque, the longitudinal force F_x acting on the tire can take positive as well as negative values as shown in Figure 18.

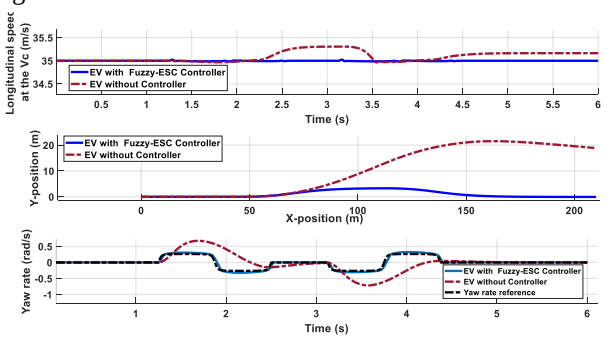

Figure 17. *Characteristics of the vehicle with Fuzzy-ESC controller compared to the vehicle without controller*

For the tire force, there is only a short-term force, corresponding to the first left turn. Furthermore, the slip coefficient and lateral slip angle are simulated as shown in Figure 18. The Fuzzy-ESC controller keeps the four tires within the safe tire grip zone with smaller layer fluctuations than the vehicle without controller. Tire number four slips and goes beyond the tire grip limit ellipse for the vehicle without electronic stability control, as shown in Figure 18 d.

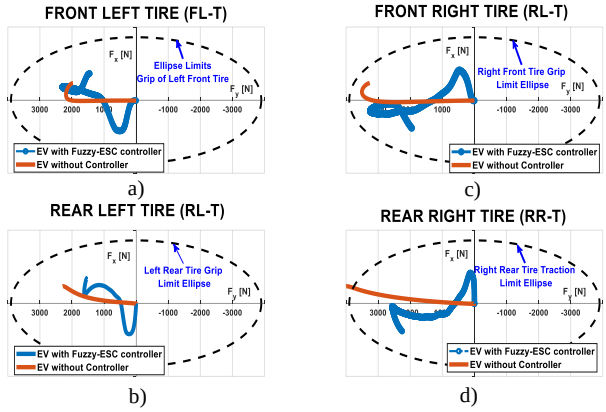

Figure 18. *Force acting on each tyre when the vehicle has a Fuzzy-ESC controller and the EVs without a controller*

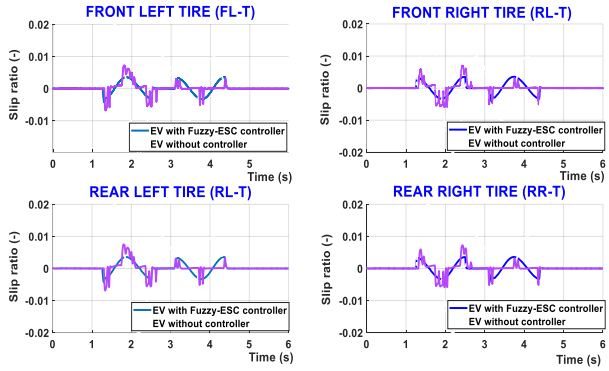

Figure 19. *Comparison of the slip coefficient of the vehicle with Fuzzy-ESC controller and the EVs without controller*

3.6. Comparison of vehicles with Fuzzy-ESC and PSO-ESP controllers

Comparison of the forces acting on the tires of four tires when the vehicle uses PSO-ESP and Fuzzy-ESC controllers is shown in Figure 20-Figure 21. From the results, we can conclude that the Fuzzy-ESC controller keeps the four tires less oscillating with better traction of the four tires, with smaller oscillations than when the vehicle uses PSO-ESP controller.

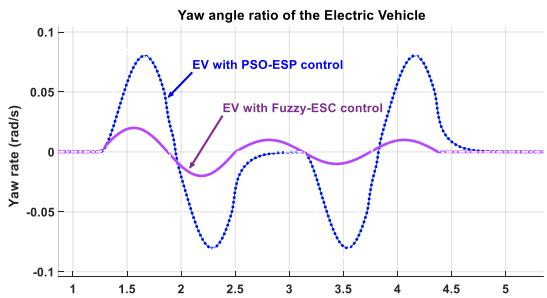

Figure 20. *Comparison of the steering angle of PSO-ESP and Fuzzy-ESC vehicles with steering angle during failure*

The performance of PSO-ESP and Fuzzy-ESC vehicles is compared. As can be seen in Figure 20 and Figure 21, all trajectories look quite similar. However, the Fuzzy-ESC vehicle can return to almost the same y-position after moving, while the PSO-ESP vehicles are shifted to the right.

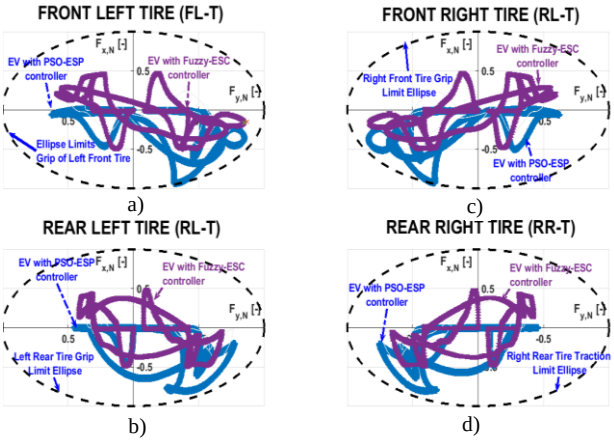

Figure 21. *Comparison of forces acting on four tires corresponding to vehicles with PSO-ESP, Fuzzy-ESC controllers*

4. Conclusions

When EVs integrate PSO-ESP or Fuzzy-ESC stability controllers, the control quality results are much better than those without controllers. Furthermore, vehicles with Fuzzy-ESC controllers have lower speed overshoot, response time and drift than those with PSO-ESP controllers. While using PSO-ESP, the longitudinal speed of the vehicle is not maintained and the tire force can approach the tire grip limit quite close to the tire grip limit because they distribute the force unevenly across the four tires. In order to maintain the longitudinal speed of the vehicle and distribute the tire force more evenly within the traction ellipse, the Fuzzy-ESC controller has a significantly better control quality, significantly improving compared to vehicles with PSO-ESP controllers

Acknowledgements: This research paper is funded by the Ministry of Education and Training under project number B2024-DHH-11.

REFERENCES

[1] Z. Wu, C. Kang, B. Li, J. Ruan, and X. Zheng. “Dynamic Modeling, Simulation, and Optimization of Vehicle Electronic Stability Program Algorithm Based on Back Propagation Neural Network and PID Algorithm”, *MDPI, In Actuators*, vol. 13, No. 3, pp.100, 2024.

[2] Z. Cheng and Z. Lu, “Research on the PID control of the ESP system of tractor based on improved AFSA and improved SA”, *Computers and Electronics in Agriculture*, vol. 148, pp. 142-147, 2018. DOI: https://doi.org/10.1016/j.compag.2018.03.013.

[3] L. A. Torres, A. Murilo, R. V. Lopes, and V. Leal, "Analysis and Virtual Validation of Vehicle Dynamics Models for Electronic Stability Control", *IEEE Latin America Transactions*, vol. 22, no. 2, pp.166-172, 2024. DOI: 10.1109/TLA.2024.10412038

[4] T. A. Nguyen, “Establishing a novel adaptive fuzzy control algorithm for an active stabilizer bar with complex automotive dynamics model”, *Ain Shams Engineering Journal*, vol.15, no.1, 102334, 2024. https://doi.org/10.1016/j.asej.2023.102334

[5] Y. Shen, Y. Zhao, H. Deng, F. Lin, and H. Shen, “Coordinated control of stability and economy of distributed drive electric vehicle based on Lyapunov adaptive theory”, *Proceedings of the Institution of Mechanical Engineers, Part D: Journal of Automobile Engineering*. vol. 238, no. 6, pp. 1535-1549, 2024. Doi:10.1177/09544070221147081.

[6] N. Wan, G. Zeng, C. Zhang, D. Pan, and S. Cai, “Multi-layer controller with state-constraint: Vehicle lateral stability control based on fuzzy logic”, *Proceedings of the Institution of Mechanical Engineers, Part D: Journal of Automobile Engineering*, vol. 236, no. 1, pp. 155-167, 2022. https://doi.org/10.1177/095440702110142

[7] A Mousaei, N. Rostami, and M. B. Sharifian, "Design a robust and optimal fuzzy logic controller to stabilize the speed of an electric vehicle in the presence of uncertainties and external disturbances", *Transactions of the Institute of Measurement and Control*, vol. 46, no. 3, pp. 482-500, 2024. https://doi.org/10.1177/0142331223117816

[8] S.D. Pande, A. Gudipalli, R. Joshi, S. Chaudhari, D. Dhabliya, S. H. Ahammad, and S. D. Kale, “A Fuzzy-Based Slip Resistive Controller for Front Wheel Drive Autonomous Electric Vehicle”, *Electric Power Components and Systems*, vol. 52, no.10, pp.1821-1831, 2024.

[9] Y. Wang, R. Lian, H. He, J. Betz, and H. Wei, “Auto-tuning Dynamics Parameters of Intelligent Electric Vehicles via Bayesian Optimization”, *IEEE Transactions on Transportation Electrification*, vol. 10, no. 3, pp. 1-15, 2023. DOI: 10.1109/TTE.2023.3346874

[10] G. Q. Geng, P. Cheng, L. Q. Sun, X. Xu, and F. Shen, “A Study on Lateral Stability Control of Distributed Drive Electric Vehicle Based on Fuzzy Adaptive Sliding Mode Control”, *International Journal of Automotive Technology*, vol. 25, no.6, pp.1415-1429, 2024.

[11] K. Koysuren, A. F. Keles, and M. Cakmakci, “Online Parameter Estimation using Physics-Informed Deep Learning for Vehicle Stability Algorithms”, in *2023 American Control Conference*. IEEE, 2023, pp. 466-471. DOI: 10.23919/ACC55779.2023.10156092

[12] D. Wu, Q. Zhang, C. Du, and Y. Li, "Path tracking and stability control of 4WID electric vehicles based on variable prediction horizon MPC", *International Journal of Vehicle Design*, vol.95, no. 3, pp.291-319, 2024. https://doi.org/10.1504/IJVD.2024.139175

[13] E. V. O. J. Kuiper, and J. J. M. Van Oosten, “The PAC2002 advanced handling tire model”, *Vehicle system dynamics*, vol. 45, no. S1, pp. 153-167, 2007.

[14] J. Liang, J. Feng, Y. Lu, G. Yin, W. Zhuang, and X. Mao, “A direct yaw moment control framework through robust TS fuzzy approach considering vehicle stability margin”, *IEEE/ASME Transactions on Mechatronics*, vol. 29, no. 1, pp.166-17, 2023. DOI: 10.1109/TMECH.2023.3274689.

[15] M. Tristano, B. Lenzo, et al, "Hardware-in-the-loop real-time implementation of a vehicle stability control through individual wheel torques", *IEEE Transactions on Vehicular Technology*, vol. 73, no. 4, pp: 4683-4693, 2024. DOI: 10.1109/TVT.2024.3364151M.

[16] B. Zhang, C. Zong, G. Chen, Y. Huang, and T. Xu, “A novel integrated stability control based on differential braking and active steering for four-axle trucks”, *Chinese Journal of Mechanical Engineering-Springer*, vol. 32, pp.1-21, 2019. https://doi.org/10.1186/ s10033019-0323-0.

[17] L. D. Hieu and I.O. Temkin, "Application of adaptive PSO and adaptive fuzzy logic controllers to speed control PMSM motor servo systems", in *MATEC Web of Conferences*, EDP Sciences, vol. 220, pp. 1-8, 2018. https://doi.org/10.1051/matecconf/201822008003.

[18] H. Wang, W. Cui, S. Lin, D. Tan, and W. Chen, “Stability control of in-wheel motor drive vehicle with motor fault”, *Proceedings of the Institution of Mechanical Engineers, Part D: Journal of Automobile Engineering*, vol. 233, no. 12, pp.3147-3164, (2019).